The International Journal of Robotics Research

A Mobile Climbing Robot for High Precision Manufacture and Inspection of Aerostructures

T. S. White, R. Alexander, G. Callow, A. Cooke, S. Harris and J. Sargent

The online version of this article can be found at:
http://ijr.sagepub.com/cgi/content/abstract/24/7/589

Additional services and information for *The International Journal of Robotics Research* can be found at:

Email Alerts: http://ijr.sagepub.com/cgi/alerts

Subscriptions: http://ijr.sagepub.com/subscriptions

Reprints: http://www.sagepub.com/journalsReprints.nav

Permissions: http://www.sagepub.com/journalsPermissions.nav

T. S. White
R. Alexander
G. Callow
A. Cooke
S. Harris
J. Sargent

Advanced Information Processing Department
BAE SYSTEMS Advanced Technology Centre
Bristol, UK
tim.white@baesystems.com

A Mobile Climbing Robot for High Precision Manufacture and Inspection of Aerostructures

Abstract

In this paper we describe the design, development, and experimental trials of a climbing robot for manufacturing and inspection applications within the aerospace industry. We describe the mechanical platform, which utilizes vacuum for attachment to vertical and over-hanging surfaces, and a traction system that enables rapid movement of the robot over planar and curved surfaces of any orientation. The main applications considered during the research were the manufacturing processes for large external surface structures such as wings and the post-manufacturing and in-service inspection of such structures. The design of suitable tool packages for manufacturing and non-destructive testing is considered in the paper. The first tool package to be implemented and tested was a five-axis high precision drill, which is described. The control system is described within this paper along with the software architecture. The software architecture for the robot was generalized, allowing different robot configurations to be described and implemented rapidly through structured configuration files. Particular attention is paid to the robot's localization and navigation system, which provides tool point precision to aircraft manufacturing tolerances. The localization system uses data from several different types of sensors and combines these with information provided by a surface model to derive six-degrees-of-freedom position and orientation using an extended Kalman filter to fuse the state information from the different sources. Tool point position is calculated through direct kinematic transformations. Improvements to this work are described, which utilize one of the initial releases of Lieca's new six-degrees-of-freedom precision measurement instruments, the Lieca LTD-800. We also summarize the experimental trials and the initial performance in terms of tool point precision and climbing performance. The concept of application of the robot and details of the technologies included in the robot that are outlined in

this paper are the subject of separate pending patent applications filed by BAE SYSTEMS plc.

KEY WORDS—mobile, climbing, robot, data fusion, extended Kalman filter, localization and navigation, manufacturing, non-destructive testing, aerospace applications

1. Introduction

The past two decades have seen a substantial amount of research into the development of mobile systems capable of moving over vertical surfaces. The main driving force for this research into climbing robots is increasing safety legislation and the economics in comparison with the alternatives. However, there has been reluctance by industry to adopt the developed climbing robots because of their lack of reliability, restricted performance, and the difficulties of operating them. The nuclear industry adopted the technology earlier than others due to the safety imperative associated with using human operators instead of robots (Collie, Luk, and White 1993; White et al. 1998). Other industries do not have such pressing safety concerns and need to have convincing economic arguments for the use of such technology. The research described in this paper aims to reduce these barriers to the adoption of the technology within the aerospace industry. It is recognized that alternative approaches have been considered for use within the aerospace industry for the applications described but have not been widely adopted (Siegel, Gunatilake, and Podnar 1998; Siegel and Gunatilake 1999; Bar-Cohen and Backes 2000; Rudlin 2002). A mobile climbing robot utilizing the adhesion and traction method described in this paper is also considered for use in the inspection of civil engineering structures by Berns and Hillenbrand (2003). Industrial plant inspection using climbing robots has been considered by Longo and Muscato (2004).

589

The system described was designed for general application in the aerospace industry. The two main applications studied were the manufacturing process for large aerostructure surfaces and non-destructive inspection for structural defects in such surfaces. The application to non-destructive examination (NDE) is considered to be the most likely to exploit the devices and techniques described within this paper in the short term.

1.1. Application Considerations

The two main applications considered were drivers for different aspects of research. The accuracy and repeatability of end-effector localization and movement were driven by the requirements of manufacturing applications. This is particularly important when component tolerances of interchangeability are considered.

The NDE applications drive the requirements for smooth motion of the device over a wide variety of surface conditions and topologies as well as reliable adhesion characteristics. It is also the opinion of the authors that the NDE applications have the most compelling business case. Consideration of this and a variety of inspection techniques are given below.

Use of the Robotic Climber in the field of non-destructive testing (NDT) is driven by airworthiness and safety considerations. This has always been an area of key importance in the aerospace industry, but due to recent trends in the utilization of airframes, its importance is increasing.

Fleets throughout the world are aging, due to the prohibitively high cost of replacements. Even the extensive fleet belonging to the United States Air Force (USAF) is slowly but surely aging. However, whilst keeping the aircraft longer avoids the upfront cost of replacement, it does not avoid the significant cost of maintaining the structure in an airworthy condition. The USAF spends over $800 million per annum maintaining its current fleet and that figure is predicted by Kinzie and Peeler (1999) to rise as the lifetimes of key systems such as the B52s are extended ever further. As the average ages of both military and civil fleets increase, the aviation authorities will demand ever greater levels of testing to ensure that the structures are safe to fly (Smith 1994).

The Federal Aviation Authority (FAA) in collaboration with US aviation industry has identified measurable inspection performance goals that would serve as guidance for the FAA's inspection activities (Galella, Flournoy, and Hughes 2002). This identification is important in so far as it defines the type, size, and location of flaws associated with an aging aircraft fleet, and serves as guidance for the development of associated NDT techniques. The overriding objective is to develop NDT methods that can reliably detect and characterize the formation of fatigue cracks in multilayer aluminum structures, to detect and characterize corrosion in hidden or inaccessible areas, and to detect and characterize disbonds and delaminations in metal and composite structures.

Traditional NDT techniques are time-consuming and frequently tedious, reducing the reliability of the data and willingness to make the measurements. However, a number of the key NDT tools could easily be adapted and improved by fitting them to a robot crawler system.

Ultrasonic, thermal, eddy current, radiographic and optical methods are the most common techniques used for detecting and characterizing corrosion. All these methods have been used, although some require large expensive facilities with limited portability because of the size and weight of detectors (e.g., radiographic methods). Given that the technique must be suitable for use on a robot, then there are limitations on the size and weight of the transducers for excitation and detection. So radiographic methods based on X-rays, neutron sources, and naturally radioactive sources would normally be ruled out.

Of the techniques, the metric by which they may be judged and ranked would be given typically by the requirement noted above, i.e., the evaluation of a thickness loss associated with corrosion. A recent study conducted on behalf of the NDE branch of the USAF Research Laboratory evaluated and ranked ultrasonic, eddy current, and thermal methods using flash lamp video thermography for the detection of corrosion in four-layer lap-joints, with a top-skin thickness of 1.6 mm (Hoppe et al. 2001). These were from a KC-135 and a Boeing 707 aircraft. Based on this evaluation, the authors concluded that conventional eddy current systems had good sensitivity to thickness loss, good spatial resolution, excellent discrimination capability, and excellent signal-to-noise ratios. The ultrasonic systems had good sensitivity to thickness loss, excellent spatial resolution, reasonable discrimination capability, and moderate signal-to-noise levels. They also concluded that the thermal wave technique had inferior capability.

The three most obvious systems that could be adapted for use on the robot crawler are: optical NDT, ultrasonic NDT, and eddy current NDT. As stated earlier in the introduction, the concept of using robots to perform NDT is not new. A number of implementations of automatic scanners and robot inspection systems are reported in the literature. These include the Automated Non-Destructive Inspector (ANDI) and the Crown Inspection Mobile Platform (CIMP; see, for example, Siegel and Gunatilake 1999), the Multifunction Automated Crawling System (MACS; see Bar-Cohen and Backes 2000), ROSTAM (Siegel et al. 1998), and ROBAIR (a European Union (EU) Craft project, "Robotic System for the Inspection of Aircraft Wings and Fuselage"). ANDI used eddy current pencil probes and a vision system, which was used mainly for navigation purposes. Siegel and Gunatilake (1999) used eddy current pencil sensors for ANDI. Although these were the state-of-the-art eddy current sensors at the time, it was concluded that more modern sensors based on linear and area arrays with computer rendition would have been more successful. CIMP used three-dimensional stereoscopic visual inspection of the aircraft surface with computer image enhancement and

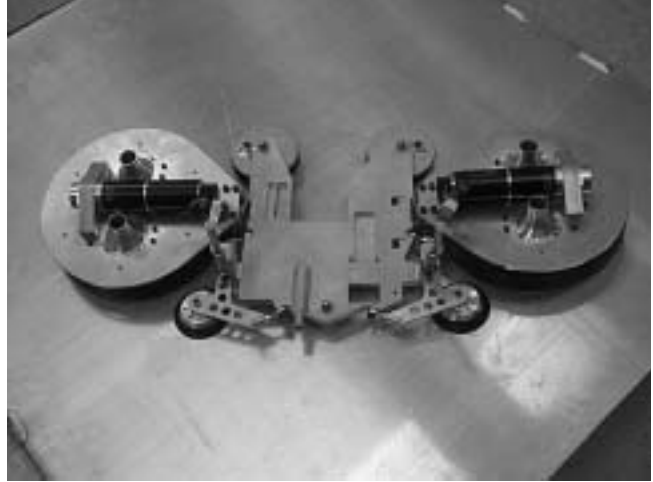Fig. 1. The robot climbing on a curved test rig.

Fig. 2. Principle features of the adhesion and traction mechanism.

automated image processing for flaw detection (Siegel and Gunatilake 1999). According to Bar-Cohen and Backes (2000), MACS was designed as a robot platform for the integration of a suite of sensors, which could include Edge-of-light, eddy current or ultrasonic sensors. The intention of MACS was to enable robot technology with open architecture computer platforms that might accommodate standard plug-in NDE boards and sensors. ROBAIR has the objective to develop an NDT inspection system based on the use of an acoustic camera, the use of a multifrequency eddy current system, a phased array ultrasonic probe with dry coupling, a thermography system, and a dry contact roller probe.

2. Mechanism Design

2.1. Adhesion and Traction

The robot adheres to the surface by using a partial vacuum developed in multiple chambers on the underside of the robot. A seal around the chambers controls the leakage of air, but is constructed to allow movement across the surface. This adhesion technique is well known and is sometimes referred to as an "inverted hovercraft". Figure 1 shows the robot climbing on a vertical curved test piece. Several important features of the system can be observed in the photograph, in particular, the robot, its umbilical and the vacuum pump. The vacuum pump used for this work was a freestanding multistage rotary vane pump, which would typically be used for industrial cleaning applications.

Motion of the robot is achieved through traction wheels mounted in the main chambers as shown in Figure 2. These provide the gross movement of the robot forwards and backwards (the X-axis), and can be operated differentially to steer the robot. As well as showing the two main adhesion chambers, Figure 2 also shows the tool package support plate, which is stabilized by three smaller vacuum chambers and two vacuum cups used to "steady" the tool when drilling takes place. The main vacuum chamber drive units and tool package support plate are connected by articulating joints, which allow the mechanism to conform to curved surfaces.

In the manufacturing application described, high precision motion is required and is provided by additional motion axes on the tool package. The chassis is designed to provide space for modular tool packages. The robot's key dimensions (LWH) are $0.5 \times 0.8 \times 0.5$ m^3 and its mass including payload is approximately 20 kg.

2.2. Localization Sensing

The primary means of providing localization data to the robot's navigation system is through the use of a Leica laser tracker. This is a high precision measurement system, which provides positional information. Figure 3 shows a photograph of the measurement head of a Lieca LTD-800; the lower part is the main tracking mechanism. It tracks a corner cube reflector (the target) using servo actuated azimuth and elevation axes to control a laser beam. An interferometer is used to measure the distance to the target; high precision optical encoders measure the azimuth and elevations angles.

A weakness of this system when used in mobile robotic applications is the narrow acceptance angle of the target. To enable the robot to move freely over the surface of the structure, the target must be turned to face the laser tracker as the robot moves. To achieve this, a servo controlled pan and tilt mechanism was developed to point the target (Figure 4). An electro-optical sensor is used to detect the laser beam striking the target and provides a control signal to orient the target coincident to the path of the laser.

Fig. 3. A Lieca LTD-800 laser tracker.
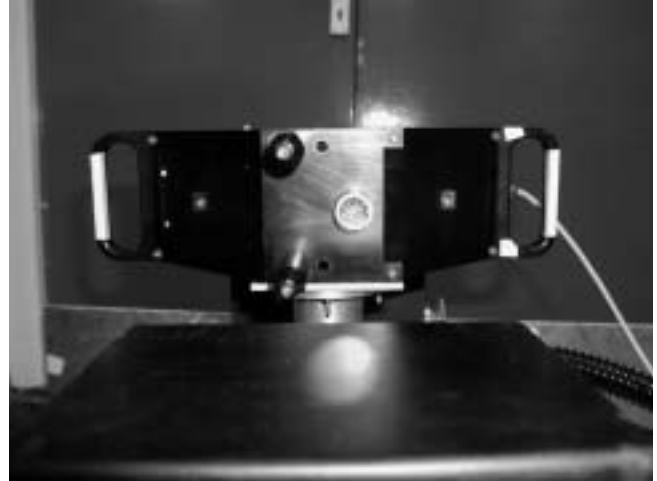
Fig. 5. LTD-800 Probe.
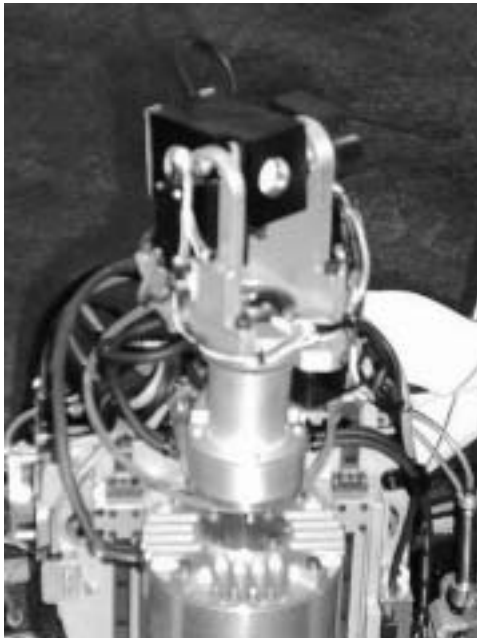
Fig. 4. Pan and tilt mechanism.

Fig. 6. Close up of drill tool package.

The current implementation of the robot, known as Crawler III (shown below), has been integrated with the new laser tracker from Lieca, the LTD-800 as part of an EU project called ADFAST. The upper part of the mechanism shown in Figure 3 is the camera system used for orientation measurement used in conjunction with a special probe, such as that illustrated in Figure 5. Orientation measurement is achieved through the use of photogrammetry. Using the combination of the camera and probe, the LTD-800 is capable of tracking a point target in full six degrees of freedom.

The probe contains a retro-reflective target for the laser beam and a series of surrounding IR light emitting diodes (LEDs) for the camera to calculate an orientation. All this can be delivered at 500 Hz. The positional accuracy of the LTD-800 is 0.02 mm and 0.02 degrees in orientation.

2.3. The Machining Tool

The first tool package developed was a cutting tool that could be used for drilling or milling operations (Figure 6). However, the application trials to date have exclusively examined its drilling capability.

The device produced could be considered to be a 5.5 axis machine tool with a bed size of 20×20 mm. The axes of movement are X, Y, Z, rot$X$, rot$Y$, and the spindle rotation. The rotational movements (rot$X$ and rot$Y$) provide the means

```
┌─────────────────────────┐            ┌─────────────────────────┐
│ Onboard PC104           │            │ Laptop PC               │
│                         │            │                         │
│ Motion Controller       │            │ Tracker Interface       │
│ Manager                 │            │ Orientation Information │
│ Read Odometry        ◄──┤  OR  ├───► │     from model.         │
│ Read Pan/Tilt angles    │            │                         │
└─────────────────────────┘            └─────────────────────────┘
            │         ┌ ─ ─ ─ ─ ─ ─ ┐              │
┌───────────────────┐ │ Pilot        │ ┌───────────────────┐
│ Motor Controllers │ │ Data Fusion  │ │ LT Controller     │
└───────────────────┘ └ ─ ─ ─ ─ ─ ─ ┘ └───────────────────┘
            │                                       │
┌───────────────────┐                   ┌───────────────────┐
│ Motor Hardware    │                   │ Laser Tracker     │
└───────────────────┘                   └───────────────────┘
```
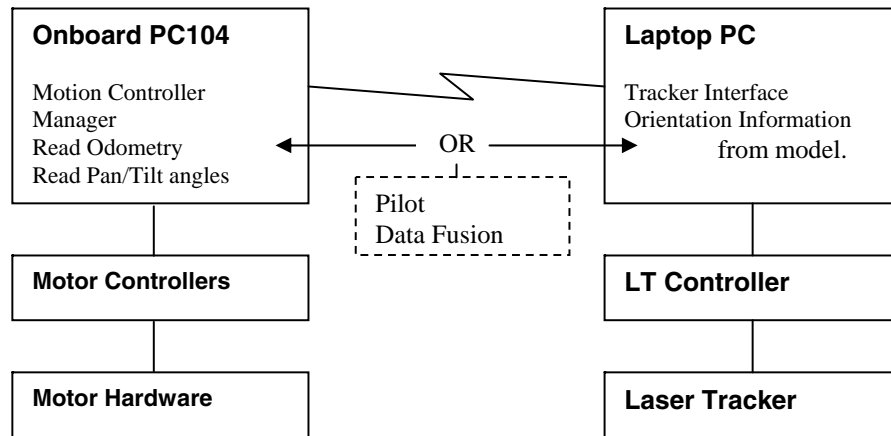
Fig. 7. Architecture diagram.

to normalize the drill angle to the surface. The axes of motion are actuated with stepper motors through lead screws to provide a high resolution of movement with very low backlash. Linear encoders provide feedback of position to the control system. An additional laser range sensor mounted on the drill and measuring the distance to the work surface is used to derive the normalization angle. A brushless AC motor with speed sensing and control powers the drill tool spindle.

3. Control System Architecture

The control architecture is designed and implemented to provide a generalized framework for other robot configurations. All the component modules are linked by remote procedure calls, allowing the control to be distributed across a number of computers with no modification. It is expected that this will be implemented using other distributed component technologies such as CORBA in the future to utilize their enhanced features. In the system described, control functions are distributed between two computers. A PC/104 stack is mounted on the robot, running an embedded version of the LINUX operating system. This stack includes the motor control cards which drive the motors, as well as providing onboard processing of sensor data. The laser tracker is connected to a laptop PC running Windows, on which the Data Fusion and Pilot modules are also usually run. The computers are connected by a wireless LAN.

The interface to the motor control hardware is implemented in a module called the Motion Controller Manager (MCM), which is structured to allow control of any configuration of mobile robot and manipulator. The robot is represented as a set of linked nodes, each of which links to either a motor axis or to a number of subsidiary nodes. A command arriving at a node can then be broken down to motions for the node's children and passed on. In the case of the Crawler, the node graph structure is currently implemented as in Figure 8.

This architecture allows any robot to be controlled using a common interface. Plug-in driver modules are used to interface to the controller hardware, and a description file indicates the layout of the robot and hence how the commands must be decomposed.

4. Localization and Navigation

4.1. Localization

In order to navigate correctly, the "pilot" must know both the robot's position (ideally, the position of its center of rotation) and its current orientation. A number of data sources are available to provide an estimate of these. In the current system, these are:

- a Leica laser-tracker unit, which produces highly accurate position information on a single point mounted atop the robot;
- feedback from a pan/tilt head, which continually faces back towards the laser tracker;
- odometric data, producing an estimate of the robot's motion.

Clearly, none of the sensors available can provide all the information required. Worse still, even when the data from the sources are combined, it is still not possible to determine the orientation of the robot fully, unless use is made of further information. In this example described CAD information on the surface can be exploited to achieve this.

It is assumed that the robot will remain at a fixed orientation relative to the surface due to the robot's fixed surface contact points. During navigation, the laser-tracker readings are used to determine the surface normal, as specified by the CAD data, of the point "underneath" the tracker target. This is assumed to be the same as the robot's local Z-axis, determining two extra degrees of freedom.
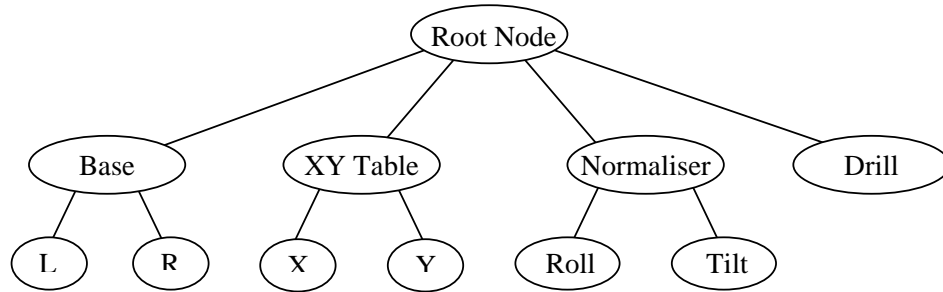
Fig. 8. Graph structure diagram.

4.1.1. Data Fusion

The measurements from the various sensors are fused using an extended Kalman filter (EKF) algorithm. This maintains an estimate of the robot's state, along with an estimate of how accurate the state estimate is in the form of a covariance matrix. The state vector describing the robot's position, orientation, rotational velocity in each axis, and (signed) speed used in the filter is as follows:

$$X = \{x, y, z, \theta_x, \theta_y, \theta_z, \theta'_x, \theta'_y, \theta'_z, v\}.$$

Each time a measurement is submitted to the Data Fusion module, a new state estimate is generated based on the old one (the predict step). In the example described, the update function is

$$X' = \begin{bmatrix} x + v \times t \times \cos(\theta_y) \times \cos(\theta_z) \\ y + v \times t \times (\sin(\theta_x) \times \sin(\theta_y) \times \cos(\theta_z) \\ + \cos(\theta_x) \times \sin(\theta_z)) \\ z + v \times t \times (\sin(\theta_x) \times \sin(\theta_z) - \cos(\theta_x) \\ \times \sin(\theta_y) \times \cos(\theta_z)) \\ \theta_x + \theta'_x \times t \\ \theta_y + \theta'_y \times t \\ \theta_z + \theta'_z \times t \\ \theta'_x \\ \theta'_y \\ \theta'_z \\ v \end{bmatrix}.$$

At the same time as the updated state is calculated, a corresponding covariance matrix is found using the standard EKF equation

$$P' = A \times P \times A^{T} + W \times Q \times W^{T}.$$

Here, Q is a covariance matrix, which adds process noise, reducing the reliance placed on old data. A and W are Jacobian matrices, which linearize the equations about the current state.

An estimate $h(X')$ is then generated of what the measurement would be if it were completely consistent with the estimated state. The estimated state covariance plus that of the measurement being submitted (R) are used to calculate the Kalman gain K:

$$K = P' \times H^{T}(H \times P' \times H^{T} + V \times R \times V^{T})^{-1}.$$

(H and V are, again, Jacobians used for linearization.) Finally, a new state estimate and state covariance are generated based on the estimate and the difference between the estimated measurement and the actual values measured:

$$X = X' + K(z - h(X'))$$
$$P = (I - K \times H) \times P'$$

where z is the measurement itself. Thus, by choosing h, H, and V to match the sensor, any relevant sensor can be fused in the filter. In the robot system described, the main sensors are the laser tracker and the pan and tilt unit. Data from wheel encoders (odometry) are also fused; however, due to the larger error associated with them, the data have a smaller effect on the final state estimate and are therefore not described in detail in this paper. The processing of data from the other sensor is described below.

4.1.2. Five-degrees-of-freedom Tracker/CAD data

The data provided by this composite sensor are as follows:

$$z = \{x, y, z, \theta_x, \theta_y\}.$$

The x, y, and z values in this measurement refer to the target on top of the robot, whereas the point of interest is its center of rotation. This complicates matters, but since rotation of the robot will be observed as a circular motion of the target, inferences can also be made on the heading of the robot from these data.

The estimated reading at each update is given by

$$h(X) = \left\{ \begin{bmatrix} x \\ y \\ z \end{bmatrix} + R \times \begin{bmatrix} C_x \\ C_y \\ C_z \end{bmatrix} \atop \theta_x \atop \theta_y \right\}$$
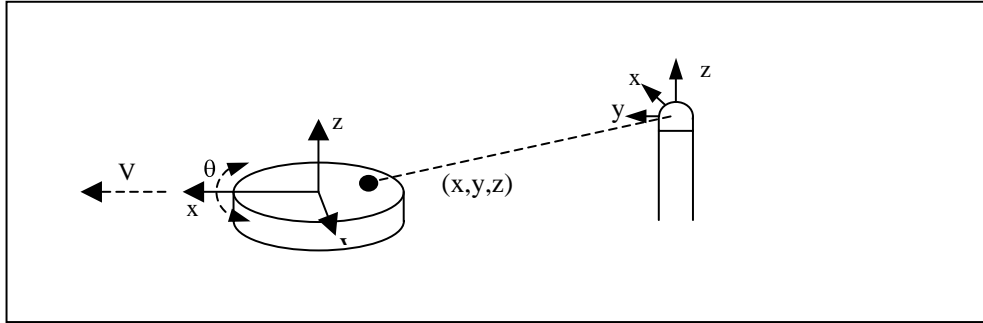
Fig. 9. Tracker and robot coordinate reference frames.
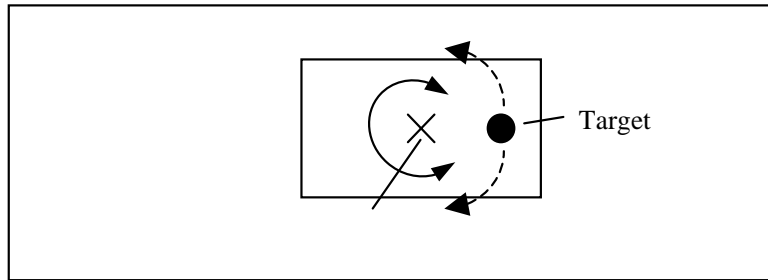
Fig. 10. Relative positions of target and centre of rotation.

where R is a 3×3 rotation matrix describing the estimated orientation of the robot. This means that when the Jacobians are calculated, differential terms are introduced that provide feedback on all the rotation angles, even without the two angles provided in the measurement. The resulting filter is capable of tracking a robot in all ten degrees of freedom contained in the state vector, even without input from further sensors. Calibration of the parameters was achieved by measurement the target during a sequence of predefined movements.

4.1.3. Pan/Tilt Data

The pan/tilt unit continually orients itself to face back towards the laser tracker. Since this is fixed at a known point in world coordinates, and the pan and tilt angles give a vector towards this point in local robot coordinates, feedback of these angles can be used to provide information on the robot's position and orientation. In particular, it allows a measurement to be made of the robot's heading, which cannot otherwise be determined directly.

The pan/tilt unit returns its value as a reading

$$z = \{\theta_y, \theta_z\}.$$

This can be derived from $V_{Trg \rightarrow Trk}$, the vector from robot to tracker, given by

$$V_{Trg \rightarrow Trk} = -V_{Trg \rightarrow R} + V_{R \rightarrow Trk}$$

where $V_{R \rightarrow Trk}$ is readily calculated from the robot's estimated position relative to the tracker, and $V_{Trg \rightarrow R}$ is a calibrated constant vector.

Defining θ_y, θ_z such that a reading of $(0, 0)$ indicates that the tracker is directly in front of the robot, this vector will form the first column of the rotation between target and tracker coordinate frames:

$$PT = \begin{bmatrix} \cos(\theta_z) & -\sin(\theta_z) & 0 \\ \sin(\theta_z) & \cos(\theta_z) & 0 \\ 0 & 0 & 1 \end{bmatrix}$$
$$\times \begin{bmatrix} \cos(\theta_y) & 0 & \sin(\theta_y) \\ 0 & 1 & 0 \\ -\sin(\theta_y) & 0 & \cos(\theta_y) \end{bmatrix}$$
$$= \begin{bmatrix} \cos(\theta_z)\cos(\theta_y) & -\sin(\theta_z) & \cos(\theta_z)\sin(\theta_y) \\ \sin(\theta_z)\cos(\theta_y) & \cos(\theta_z) & \sin(\theta_z)\sin(\theta_y) \\ -\sin(\theta_y) & 0 & \cos(\theta_y) \end{bmatrix}.$$

Normalizing $V_{Trg2Trk}$, and abbreviating it as V, our estimate then becomes

$$h(X) = \left\{ \begin{array}{c} \theta_y \\ \theta_z \end{array} \right\} = \left\{ \begin{array}{c} \arcsin(-V_z) \\ \arctan\left(V_y / V_x\right) \end{array} \right\}.$$

Again, the resulting Jacobians are large, but the ability to directly measure orientation makes the navigation task much simpler than would otherwise be the case.

4.1.4. Development of Localization and Coordinate System Transformations

Localization of the platform is relatively straightforward, as all degrees of freedom are available. The original version of the robot had to infer orientation parameters from other sensors, which included an onboard odometer and readings from a pan/tilt device. The robot was developed further to improve localization, making use of the Lieca LTD-800

The data available to the robot from the measurement of the probes position and orientation consist of the position (x, y, z) value plus a quaternion $(q0, q1, q2, q3)$ value and Euler (omega, phi, kappa) angles. From these values the coordinate transformation was built up. As part of the improvements to the system, quarternion representations were used. Quaternions are the preferred measure of orientation due to the disadvantages of singularities with Euler angles. The coordinate transform, which describes how to move between the base coordinate system of the tracker and the probe, is represented as a 4–4 homogenous matrix and is constructed as follows:

$$Tr\_to\_Probe = \begin{bmatrix} 1 - 2(q2^2 - q3^2) & 2(q1q2 - q3q0) \\ 2(q1q2 + q3q0) & 1 - 2(q1^2 + q3^2) \\ 2(q1q3 - q2q0) & 2(q2q3 + q1q0) \\ 0 & 0 \end{bmatrix}$$

$$\begin{bmatrix} 2(q1q3 + q2q0) & x \\ 2(q2q3 - q1q0) & y \\ 1 - 2(q1^2 + q2^2) & z \\ 0 & 1 \end{bmatrix}.$$

Calculation of the transformation that transforms the axes of the probe onto the axes of the drill is needed in order to calculate the location of the drill in laser-tracker coordinates. This transform called *Probe_to_Drill* is fixed as the probe is mounted on the index table. The transform is calculated first by measuring the location of the probe (*Tr_to_Probe*). Secondly, a small retro-reflective target is attached to the index table and moved to different locations while measuring the readings from the tracker of the target. This describes a transform, *Tr_to_RetroTarget*. The origin of this coordinate system is the location of the retro-reflector in tracker coordinates. These axes then need to be moved onto the drill tip. The offset between the position of the retro-reflector and the drill tip is highlighted in Figure 11.

The offset is measured by inscribing a circle around the drill tip using the target and measuring with the laser. A best-fitting circle is made to the points taken. This point $(x, y, z)_{Drill}$ is the location of the drill tip in tracker coordinates. The location of this point in the *Tr_to_RetroTarget* coordinate system is

therefore

$$(x, y, z)_{offset} = Tr\_to\_RetroTarget^{-1} \cdot (x, y, z)_{Drill}.$$

Expressed as a transformation, *RetroTarget_to_Drill*

$$RetroTarget\_to\_Drill = \begin{bmatrix} 1 & 0 & 0 & x_{offset} \\ 0 & 1 & 0 & y_{offset} \\ 0 & 0 & 1 & z_{offset} \\ 0 & 0 & 0 & 1 \end{bmatrix}$$

Probe_to_Drill is then

$$Probe\_to\_Drill = (Tr\_to\_Probe)^{-1}$$
$$\times \ Tr\_to\_RetroTarget$$
$$\times RetroTarget\_to\_Drill.$$

For any on-line probe measurement, $Tr\_to\_Probe_{online}$, the location of the drill in laser coordinates can be calculated. This point can be transformed into drill coordinates by applying the inverse transform:

$$Drill\_to\_Tr = (Tr\_to\_Probe_{online} \times Probe\_to\_Drill)^{-1}. \quad (1)$$

The location of the drill waypoint is measured in tracker coordinates and is transformed into drill coordinates using the transform in eq. (1). The locations of the drill and corresponding waypoint are now known in the drill coordinate system. Given that the robot is capable of only two-dimensional movement, using simple trigonometry a distance and bearing calculation is made to the waypoint.

4.2. Navigation

The second part of the navigation system uses the results produced by the data fusion system to pilot the robot. This module accepts sets of waypoints, and then uses a fairly simple navigational strategy to position the robot's tool over each waypoint in turn.

The basic algorithm followed by the navigation thread is as follows.

- The current state estimate is retrieved from the data fusion module.

- The waypoint position is recalculated relative to the robot, and projected onto the local plane (reducing the problem to the two dimensions in which the robot can actually move).

- If the robot is in position, drill; otherwise, move the robot or tool. Within the range of the *XY* table, the required motion is simply the vector from tool to target in local coordinates. Otherwise, the target is beyond *XY* table range, and the robot must be moved.

Drill Tip

Retroreflective
Target

Fig. 11. Retro-reflective target.

Representing the robot's motion as the matrix M, and the transform from robot to tool as T, the tool position after a motion will be M × T. The required robot motion can then be represented as M × T = W where W is the waypoint to be drilled.

M is a rotation about z (θ) combined with a translation in x (d), so the above equation reduces to two simultaneous equations:

$$T_x \cos(\theta) - T_y \sin(\theta) + d = Trg_x$$
$$T_x \sin(\theta) + T_y \cos(\theta) = Trg_y.$$

These can readily be solved for θ and d, producing two possible motions. The robot can turn to face the target and move forwards, or turn away and reverse. The solution to use is chosen to avoid tangling the robot up in its own hose, by ensuring that the back of the robot always faces roughly in the same direction. The required steering angle and speed are determined from the above angle and distance.

5. Trials and Results

The trials conducted to date have included movement and adhesion on various surface topologies and orientations as well as drilling accuracy and repeatability. The results for the initial testing gave drilling position repeatability of ±0.2 mm. Accuracy seems to be of a similar order on flat surfaces. The development of position and orientation described improved this performance and the test results on a flat vertical panel achieved an accuracy of 6 mm for coarse navigation and ±0.1 mm for final accurate navigation.

Trials and results of experiments to measure the performance improvements of the LTD-800 are described by Kilhmann, Loser, and Cooke (2004). In this case, they describe the performance of the LTD-800 integrated with an ABB robotic arm for drilling trials. These experiments achieved an accuracy of 0.05 mm in position and 0.04 degrees for orientation. The research described in Kilhmann, Loser, and Cooke (2004) is directly related to the research described in this paper, and represents the limits of localization performance of the climbing robot described within.

The robot demonstrated reliable climbing performance on all orientations of a 1.5 m radius cylindrical surface including complete inversion while carrying a 12 kg payload. An initial application trial has also been completed to provide a concept demonstration of skin drilling on a large aerospace structure. The results have shown that the robot could be used for the application; however, further development is required to increase drill sequence cycle times.

6. Conclusions

The mechanism described offers several performance advantages over alternative climbing robots, which use stepping motions such as those described in Collie, Luk, and White (1993) and White et al. (1998). First, the robot produces smooth continuous motion, which enables fast efficient coverage of the climbing surface. The traction mechanism is at its simplest a pair of driven wheels, the complexity of stepping is not required and therefore the number of moving parts is substantial reduced thus improving reliability. The simplicity of the traction mechanism also reduces the need for the elaborate control systems required to provide smooth, safe, stepping motions, and thus will help to address perceptions of the robustness of the approach with the user community

The localization sensors described were selected to enable the highest potential precision and accuracy to enable the widest possible application of the systems. While these approaches do provide precision, they also require a direct line of sight between the robot and the laser tracker. This can easily be arranged in many cases, but will ultimately limit use in applications where the climbing surfaces and supporting structure are complex.

The robot's performance to date has provided substantial evidence of the suitability of the technologies developed for many applications within the aerospace industry. The most immediately applicable are the NDT applications for which high resolution and accuracy to the level described are not needed. In many cases, ±5 mm localization is adequate and therefore other approaches to localization are possible

including video photogrammetry without the need for laser trackers. Other applications such as skin drilling are also achievable in the short term. However, we acknowledge the need to continue the research in this area to develop accuracy, speed, and robustness of the system as well as the development of tool packages for different applications.

Acknowledgments

References

Bar-Cohen, Y. and Backes, P. 2000. Scanning large aerospace structures using open-architecture crawlers. National Space and Missile Materials Symposium, San Diego, CA, February 27–March 2, http://eis.jpl.nasa.gov/ndeaa/ndeaa-pub/MACS/MACS-NSMMS-2000.pdf.

Berns, K. and Hillenbrand, C. 2003. A climbing robot for inspection tasks in civil engineering. ASER03 1st International Workshop on Advances in Service Robotics, Bardolino, Italy, March 13–15.

Collie, A. A., Luk, B. L., and Whire, T. S. 1993. Climbing robots for the nuclear industry. *Proceedings of the International Conference on Remote Techniques for Nuclear Plants*, BNES, Stratford, UK.

Galella, D., Flournoy, T., and Hughes, W. J. 2002. FAA sponsored non-destructive inspection research. http://www.arofe.army.mil/Conferences/NDE-workshop/Flournoy.pdf.

Hoppe, W., Pierce, J. L., Ko, R., Schehl, N., and Buchanan, D. 2001. Results from the hidden corrosion detection evaluation on the automated corrosion detection program probability of detection. Proceedings of the 5th Joint NASA/FAA/DoD Conference on Aging Aircraft, Orlando, FL, September 10–13 (http://www.agingaircraft2001.com/papers/IndexPDFs/6B_1.pdf).

Kilhmann, H., Loser, R., and Cooke, A. 2004. Metrology-integrated industrial robots—calibration, implementation and testing. Proceedings of the 35th International Symposium on Robotics, Paris, France, March 23–26.

Kinzie, R. and Peeler, D. 1999. Managing corrosion in the aging fleet: a new approach to corrosion maintenance. Proceedings of the 3rd Joint Conference on Aging Aircraft, Albuquerque, NM.

Longo, D. and Muscato, G. 2004. A modular approach for the design of the Alicia3 Climbing Robot for industrial inspection. *Industrial Robot Journal* 31(2):148–158.

Rudlin, J. 2002. ROBAIR project. *In Service Structural Integrity and Repair*, May 30, IMechE, Bristol.

Siegel, M. and Gunatilake, P. 1999. Robotic enhanced visual inspection of aircraft skin, http://voronoi.sbp.ri.cmu.edu/∼fsr/FINAL_PAPERS/33_Seigel.pdf.

Siegel, M., Gunatilake, P., and Podnar, G. 1998. Robotic assistants for aircraft inspectors. *IEEE Instrumentation and Measurement Magazine* 1(1):16–30 (http://www-2.cs.cmu.edu/afs/cs/project/sensor-9/ftp/papers/imm97.pdf).

Smith, R. A. 1994. Non-destructive evaluation for corrosion in aging aircraft. DRA/SMC/TR941004, September.

White, T. S., Hewer, B., Luk, B., and Hazel, J. 1998. Design and operational performance of a climbing robot used for weld inspection in hazardous environments. IEEE Control Applications Conference, Trieste, Italy.